Pancreatic cancer cells overexpressing interleukin 6 induce T-cell-mediated tumor clearance and durable anti-tumor immune response

Paige C. Arneson-Wissink[1], Alexandra Q. Bartlett[2], Heike Mendez[1], Xinxia Zhu[1], Jessica Dickie[1], Matthew McWhorter[2], Peter R. Levasseur[1], Parham Diba[1], Katelyn T. Byrne[3,4], Gregory D. Scott[5], Robert Eil[2], Aaron J. Grossberg[1, 4, 6]*

[1] Department of Radiation Medicine, Oregon Health & Science University, Portland, OR, 97239, USA
[2] Division of Surgical Oncology, Department of Surgery, Knight Cancer Institute, Oregon Health & Science University, Portland, OR, 97239, USA
[3] Department of Cell, Development, and Cancer Biology, Oregon Health & Science University, Portland, OR, 97239, USA
[4] Brenden Colson Center for Pancreatic Care, Oregon Health & Science University, Portland, OR, 97239, USA
[5] Department of Pathology, Oregon Health & Science University, Portland, OR, 97239, USA
[6] Cancer Early Detection Advanced Research Center, Oregon Health & Science University, Portland, OR, 97201, USA

***Corresponding Author**: Aaron J. Grossberg, 3181 SW Sam Jackson Park Rd Mail Code L481, Oregon Health and Science University, Portland, OR, 97239, 503-494-9945, grossber@ohsu.edu

Conflict of interest: RE is a paid consultant and conducts ongoing research for Lyell Immunopharma. KTB receives consultation feed from Guidepoint Global and royalties from the University of Pennsylvania for licensed research cell lines. The other authors declare no conflicts.

ABSTRACT

Tumor immune resistance is recognized as a contributor to low survivorship in pancreatic ductal adenocarcinoma (PDAC). We developed a novel murine model of spontaneous PDAC clearance, generated by overexpressing interleukin-6 (IL-6) in orthotopically implanted PDAC cancer cells (OT-PDAC^{IL6}). Circulating IL-6 was 100-fold higher in OT-PDAC^{IL6} than in OT-PDAC^{parental} mice. OT-PDAC^{IL6} tumors were present at 5 days post-implantation, and undetectable by 10 days post implantation. Flow cytometry revealed increased T cells and NK cells, and decreased T regulatory cells in OT-PDAC^{IL6} as compared to OT-PDAC^{parental} tumors. Increased lymphoid aggregates were apparent by histological assessment and may account for elevated T cell content. Antibody-based depletion of CD4^{+} and CD8^{+} T cells prevented tumor clearance and significantly reduced survival of OT-PDAC^{IL6} mice. The anti-tumor immune response to OT-PDAC^{IL6} rendered mice immune to re-challenge with OT-PDAC^{parental} tumors. In high concentrations, IL-6 acts in opposition to previously described pro-tumorigenic effects by enhancing the T cell-mediated anti-tumor response to PDAC.

Statement of Significance: Interleukin 6 overexpression in pancreatic ductal adenocarcinoma cells induces T cell-driven tumor clearance that is rapid and durable. Supraphysiologic levels of interleukin 6 are sufficient to drive an anti-tumor immune microenvironment hallmarked by increased lymphoid aggregate formation, increased CD4 T cell abundance, and decreased Treg abundance.

Key words: Interleukin 6, Pancreatic Ductal Adenocarcinoma, T-cell response

INTRODUCTION

Interleukin-6 (IL-6) signaling is associated with reduced survival in patients with pancreatic ductal adenocarcinoma (PDAC), attributed to the promotion of metastasis, tumorigenesis, and cachexia[1-4]. Published literature shows that loss of IL-6 attenuates PDAC development, cachexia onset, and metastasis [5-7]. We previously demonstrated that host intrinsic IL6 signaling was necessary to develop PDAC cachexia[6]. To extend this finding, we sought to ask if IL6 overexpression in cancer cells would be sufficient to restore cachexia in an otherwise IL6 deficient host. We developed stable IL-6 overexpressing PDAC cells ($PDAC^{IL6}$) from the $PDAC^{parental}$ cell line (KxPxCx) [8] using ecotropic retroviral transduction. We found that $PDAC^{IL6}$ cells produced extremely high levels of IL-6 and induced severe cachexia within days of orthotopic implantation (OT-$PDAC^{IL6}$). Despite this, we observed unexpected and dramatic changes in tumor growth dynamics, culminating in complete tumor clearance and long-term, recurrence-free mouse survival. We then pursued a series of studies to understand the mechanistic underpinnings of tumor clearance in our model, focusing on the immune response to high intra-tumoral IL-6. Our work presents a previously undescribed ability for IL-6 to induce T cell-mediated PDAC tumor clearance. Typically, PDAC is associated with an immunosuppressive microenvironment, which limits the efficacy of immunotherapies in treating PDAC [9,10]. Increased T-cell infiltration is associated with improved survival and strategies to increase T-cell activation and infiltration benefit mouse survival in pre-clinical models [11,12]. The work shown here presents IL-6 over-expression as a novel mechanism by which PDAC tumors experience more T cell infiltration and are poised for a favorable anti-tumor immune response.

METHODS

Mouse Studies

74 *Husbandry*

75 C57BL/6J (WT, JAX 000664) mice were purchased from The Jackson Laboratory (Bar Harbor,
76 ME) and maintained in our animal facility. All mice were housed and bred in a dedicated
77 mouse room maintained at 26 °C, 40% humidity, and 12-h light/dark cycle. Mice were provided
78 *ad libitum* access to food and water (5L0D, PicoLab) unless otherwise stated. All mice were 12
79 weeks of age at experiment start. Sex in each experiment is defined in the figure legends.
80 When single housed, mice were allowed a 7 day acclimation period prior to procedure/study
81 start. All tumor studies followed humane endpoints. All mice were humanely euthanized via
82 cardiac puncture or cervical dislocation under deep isoflurane anesthesia. Mouse studies were
83 conducted in accordance with the NIH Guide for the Care and Use of Laboratory animals, and
84 approved by the Oregon Health & Science University IACUC.

85 *Orthotopic Tumor Implantation*

86 A vial of frozen KPC cells was thawed prior to each implantation, and 1 million cells were
87 implanted in 23 uL of PBS per mouse. All mice were anesthetized with isoflurane, scrubbed
88 with betadine, and a para-midline incision was made in the abdomen to expose pancreas. KPC
89 cells or vehicle (PBS) were injected directly into the pancreatic parenchyma. Pancreas was
90 placed back into position and incision was closed using two sutures (4-0 Polysorb) and two
91 skin staples.

92 Subcutaneous Tumor Implantation

93 A vial of frozen KPC cells was thawed prior to each implantation, and 1 or 2 million cells were
94 implanted in 100 uL of PBS per mouse. The mouse's lower right abdomen was shaved, then
95 the needle was inserted near the right 4th mammary gland.

96 *IVIS imaging*

97 Mice were injected with 100 uL of 15 mg/mL D-luciferin potassium salt in DPBS (no Ca, no Mg)
98 (GoldBio, #LUCK-100), then anesthetized with isoflurane. 10 minutes later, a luminescent
99 image and photo were captured. Longitudinal data was analyzed in one batch by normalizing
100 tumor ROI luminescence total counts to average background ROI luminescence total counts.

101 *Antibody-based depletion*

102 Mice were dosed intraperitoneally (IP) with either a combination of CD4 (BioXcell, #BE0003-1)
103 and CD8a (BioXcell, #BE0061) depletion antibodies, or Rat IgG2b isotype control antibody
104 (BioXcell, #BE0090), which were resuspended in InVivoPure ph7.0 Dilution Buffer (BioXcell,
105 #IP0070) per the manufacturer's instructions. First dose was 0.2 mg each antibody per mouse,
106 given IP two days prior to tumor implantation. Following doses were 0.1 mg each antibody per
107 mouse, given IP every 4 days after initial dose.

108 ***Cell lines***

109 *Growth Conditions and validation*

110 All cells were maintained at 37°C and 5% CO_2 in a humidified incubator, and tested negative in
111 house for mycoplasma using Universal Mycoplasma Detection Kit (30-1012K). *Kras*$^{G12D/+}$,
112 *Tp53*$^{R172H/+}$, *Pdx1-Cre* (KPC) cell line was generously shared by Dr. Elizabeth Jaffee[8,18]. KPC
113 cells were grown on tissue culture-treated dishes in growth media consisting of RPMI (Gibco)
114 with 10% FBS (Corning) and 1% penicillin/streptomycin (Gibco).

115 *Engineered KPC*

116 KPC cells expressing the surface marker Thy1.1 (CD90.1) with blasticidin resistance (BSR),
117 IL-6 with puromycin resistance, and luciferase with hygromycin resistance, were generated
118 from our stock of KPC cells (female) described above. IL-6 sequence was codon-optimized for
119 efficient expression (**Figure S9**). Platinum-E ecotropic packaging cells were transfected with

120 plasmid DNA encoding MSGV-Thy1.1, MSGV-IL6-Puro, or MSGV-Luciferase as described
121 previously[19]. Retroviral supernatants were spiked with 2ug/mL polybrene and were mixed 1:1
122 with fresh media before adding to 6-well tissue culture treated plates. Cells were spun at
123 2000g for 90min, 32C, no brake. Cells were then incubated at 37C for 48 hours before
124 washing off the viral supernatant and adding DMEM media (Gibco) supplemented with 10%
125 FBS (Corning). Two days later, KPC cells were placed in complete DMEM media containing
126 puromycin (5ug/mL) and/or blasticidin (5ug/mL) and/or hygromycin (500 ug/mL) to select for
127 transduced cells. Following antibiotic selection, successful transduction was confirmed via flow
128 cytometry staining for Thy1.1. KPC-CD90.1, KPC^{IL6}, and KPC^{LUC} cells were implanted for OT-
129 PDAC as described for parental KPC cells. Continued culturing of engineered cells was done
130 in selection media described.

131 ***Flow cytometry***

132 *Brefeldin A injections:* For intracellular cytokine staining for flow cytometry, we followed
133 previously published protocols for golgi transport blockade[20]. Briefly, each mouse received
134 100ug Brefeldin A (Selleckchem) injected retro-orbitally 5 hours prior to tissue collection.

135 *Sample preparation*

136 We collected tumors from mice 5 days post implantation, and tumors were weighed, then
137 placed in PBS on ice. Tumor tissue was minced and digested (7). After dissociation, we
138 strained tumor suspension through at 100 um filter, and performed ACK lysis. We collected
139 spleens from mice at the endpoint specified. Spleens were pressed through a 70 um filter,
140 rinsed with PBS, pelleted at 1500 RPM for 5 minutes, and lysed with ACK lysis.

141 *Staining*

142 We stained samples with live/dead stain (1:2000) and surface protein antibodies (1:200 each),

143 and incubated for 20 minutes room temperature (**Table S3**). After staining, we washed
144 samples with FACS buffer and pelleted. For intracellular staining (Foxp3), we fixed and
145 permeabilized cells with 4% paraformaldehyde (BD Cytofix/Cytoperm), washed cells, and then
146 resuspended cells in antibody diluted 1:200 in permeabilization buffer (BD Perm/Wash) with
147 overnight incubation at 4C . The next day we washed and resuspended cells with FACS buffer
148 prior to analysis.

149 *Instrumentation and analysis*

150 All samples were analyzed in the OHSU Flow Cytometry Shared Resource using the Cytek
151 Aurora flow cytometer (Cytek Biosystems), data was analyzed in FlowJoTM v10.8.1. Samples
152 were first gated according to size and single cells, then all live cells were captured. The live
153 population was gated on CD45+ cells to capture all leukocytes. To identify T cells, leukocytes
154 were gated on CD90.2 then sub-gated for CD4+ or CD8+ cells. The CD4+ T cell population
155 was gated on Foxp3 to assess T regulatory cells. Natural killer (NK) cells were sub-gated from
156 the parental CD45+ gate. All NK1.1+ cells were captured, and then divided by expression of
157 CD90.2 to classify as NK (conventional, CD90.2-) or NK T cells (CD90.2+).

158 ***Histology***

159 Pancreas/tumor tissue was fixed overnight in 4% PFA, then stored in 70% ethanol. Tissues
160 were paraffin embedded, sectioned, and hematoxylin and eosin (H&E) stained by the OHSU
161 Histopathology Shared Resource. Tumor tissue was sectioned in 5um slices at levels 50 um
162 apart. H&E stained tumor cross-sections were evaluated by a board-certified gastrointestinal
163 pathologist. All samples were blinded during sectioning/staining and during evaluation. 3-5
164 depths of tissue were qualitatively assessed per mouse. For day 5 tumor samples, 2 depths of

165 tissue were quantified per mouse and averaged together. For day 12 tumor samples, 1 section
166 was quantified.

167 ***Immunofluorescent staining and quantification***

168 Pancreas/tumor tissue was dissected, transferred to BD Cytofix/Cytoperm diluted to 1% PFA,
169 and kept at 4C overnight. Tissue was then transferred to 30% sucrose in PBS and kept at 4C
170 overnight. Tissue was then washed twice in PBS before embedding in OCT media (Sakura).
171 Tissue was cut at 8 um onto superfrost plus slides and stored at -80C until staining. To stain,
172 slides were washed with PBS, blocked with 2.5% BSA 0.3% TritonX in PBS for one hour,
173 stained with pre-conjugated antibodies (**Table S3**) for 1h, washed with PBS, quenched with
174 TrueView Autofluorescence Quench kit (Vector, SP-8400) 2-5 min, stained with DAPI diluted
175 1:1000 for 10 min, and mounted with Vectashield Vibrance mounting medium (Vector, H-
176 1700). Whole tissue sections were imaged on a Zeiss Axio Scan 7 at 20x magnification. Two
177 tissue sections at least 344 um apart were assessed per sample. All images were blinded prior
178 to annotation and analysis. In QuPath (V0.5.1), areas of tumor, as defined as PanCK positive,
179 and stroma, as defined as PanCK negative abnormal tissue, were annotated. Adjacent tissue
180 sections were stained with H&E and used as reference for areas of stroma. Annotations were
181 made using only the DAPI and PanCK stains. After annotation, $CD3^+$ cells ($CD3^+$, $DAPI^+$,
182 PanCK-) were manually counted in stroma and tumor areas. Final counts were normalized to
183 total area of stroma or tumor annotation.

184 ***Plasma analytes***

185 Plasma was collected, snap frozen in liquid nitrogen, and stored at -80ºC. Plasma
186 concentrations of IL-6 (Biolegend) were measured using ELISA, and read on a plate reader
187 (BioTek).

188 ***Quantitative real-time polymerase chain reaction (qPCR)***

189 We isolated RNA from cell pellets or tissue samples using the E.Z.N.A. Total RNA Kit I
190 (Omega BioTek), and we prepared cDNA using a high-capacity cDNA reverse transcription kit
191 (Applied Biosystems). qPCR was run on the ABI 7300 (Applied Biosystems), using TaqMan
192 Fast Advanced PCR master mix (Applied Biosystems) or SYBR Green master mix (Applied
193 Biosystems). Relative expression was calculated using the $\Delta\Delta C_t$ method. To confirm the
194 presence/absence of *Il6 transgene* in tumor-implanted mice, we performed 30 cycles of qPCR
195 on the ABI7300, followed by running the PCR product on a 3% ethidium bromide gel to
196 determine the presence of a band at the expected size of 131 bp. Primers/probes are listed in
197 **Table S2**.

198 ***Statistical Analysis***

199 Specific statistical tests and sample sizes for each study are indicated in the figure legends.
200 Error bars in the figures show SEM. Statistical analyses were performed using GraphPad
201 Prism (version 9; GraphPad Software Inc) or JMP Pro (version 16; SAS Institute Inc), and
202 graphs were built using GraphPad Prism (GraphPad Software Inc) statistical analysis software.
203 P values are two-sided, with values less than 0.05 regarded as statistically significant.

204 ***Data Availability***

205 Further information and resources, including plasmid sequences, engineered KPC cells, and
206 raw data, will be shared upon reasonable request to Aaron J. Grossberg
207 (grossber@ohsu.edu).

208 **RESULTS**

209 **Tumor-specific IL6 overexpression induces spontaneous tumor clearance and cachexia**
210 **recovery.** We developed $PDAC^{IL6}$ and control-transduced $PDAC^{CD90.1}$ cells from the

211 PDAC^{parental} (KxPxCx, [8]) using ecotropic retroviral transduction. Histological assessments of
212 tumors showed that both OT-PDAC^{IL6} and OT-PDAC^{parental} developed poorly differentiated,
213 infiltrative carcinoma by five days (**Figure 1A-C**). OT-PDAC^{IL6} tumors were slightly smaller in
214 mass and histological area than OT-PDAC^{parental} tumors (**Figure 1C-D**). By 12 days, OT-
215 PDAC^{parental} and OT-PDAC$^{CD90.1}$ mice had reached humane euthanasia endpoint, with
216 carcinoma covering approximately 80% of total tissue area, in contrast, OT-PDAC^{IL6} tissue was
217 completely devoid of tumor, and mice had regained all bodyweight lost during tumor growth
218 (**Figure 1B, D-E, I, Figure S1A-D, Table S1**). We confirmed this result molecularly using
219 qPCR for the codon-optimized *Il6* transgene, which was not detected in OT-PDAC^{IL6} whole
220 pancreas tissue after five days (**Figure 1F, Figure S2A-D**). While lung and liver metastases
221 were detected by *Il6* transgene qPCR at five days, there were no metastases detected at 12
222 days (**Figure S3A-D**). Spontaneous tumor clearance also occurred when PDAC^{IL6} cells were
223 implanted subcutaneously, indicating that the phenomenon is not specific to intrapancreatic
224 administration (**Figure S4A-C**). IL-6 overexpressing models generated from alternative PDAC
225 cell lines also displayed increased survival and decreased tumor burden relative to parental
226 lines, although we did not observe complete tumor resolution in the other cell lines (**Figure**
227 **S5A-F**).

228 To assess the cachexia phenotype and general mouse health, we measured plasma IL-6, a
229 known contributor to cachexia development. OT-PDAC^{parental} plasma IL-6 levels were in line
230 with previously published values, while OT-PDAC^{IL6} levels reached 100-fold higher levels at
231 day 5, followed by undetectable levels at later time points (**Figure 1G**) [3,6]. Spleens from OT-
232 PDAC^{IL6} mice were significantly enlarged, consistent with systemic inflammation elicited by
233 high circulating IL-6 levels (**Figure 1H**). High plasma IL-6 and peak tumor burden also

234 associated with decreased body mass, which recovered with the normalization of IL-6 (**Figure**
235 **1I**). Gross muscle and adipose tissue mass trended downward at five days and were
236 significantly decreased at 12 days, reflecting a delay in tissue recovery as the tumor resolves
237 and body mass returns to baseline (**Figure 1J-L**). Collectively, these data show that IL-6
238 overexpression in PDAC cells leads to severe wasting, followed by spontaneous tumor
239 resolution.

240 **OT-PDAC^{IL6} induces lymphocytic anti-tumor immune response.** We hypothesized that the
241 extreme levels of IL-6 generated in the pancreas of OT-PDAC^{IL6} mice facilitated immune-
242 mediated tumor clearance. We used flow cytometry to evaluate the immune profile of OT-
243 PDAC^{IL6} and OT-PDAC^{parental} tumors and discovered that pancreata bearing OT-PDAC^{IL6}
244 tumors were enriched with CD4^{+} T cells and Natural Killer (NK) cells, while Foxp3^{+} T-
245 regulatory cells were decreased (**Figure 2A-E, Figure S6A-C**). Because increased tumor-
246 infiltrating lymphocytes are associated with improved outcomes and therapeutic efficacy, we
247 next assessed the localization of T cells relative to tumor[12]. By immunofluorescent staining, we
248 found that OT-PDAC^{parental} and OT-PDAC^{IL6} mice had equal densities of CD3^{+} T cells in both
249 tumor-associated stroma and tumor nests (**Figure 2F-H**). These data were initially
250 contradictory to the flow cytometry data. However, upon histological assessment, we found
251 that OT-PDAC^{IL6} pancreata exhibited a significantly greater number of tumor-associated
252 lymphoid aggregates (**Figure 2I-J**). In PDAC, lymphoid aggregate formation is associated with
253 improved survival[13,14]. In OT-PDAC^{IL6} mice, the lymphoid aggregates were often near, but not
254 necessarily located within the tumor stroma, which accounts for the differences between our
255 flow cytometry and immunofluorescence data. In summary, locally high IL-6 induces
256 accumulation of lymphoid aggregates, increased CD4^{+} T cells, and decreased Foxp3^{+} T

257 regulatory cells. These conditions favor the hypothesis that tumor clearance occurs via an anti-
258 tumor T cell response.

259 **T cells are necessary for OT-PDAC^{IL6} tumor clearance**. Based on our flow cytometry
260 analysis, we hypothesized that T cells are necessary for OT-PDAC^{IL6} tumor clearance, which
261 we tested using CD4 and CD8 depletion antibodies, compared to IgG control treatment. Mice
262 received antibody injections two days before tumor implantation and every four days following.
263 We followed humane endpoints for the CD4/CD8-depleted group, which reached euthanasia
264 criteria at 8-11 days post-implantation (**Figure 3A**). We euthanized all sham and IgG-treated
265 mice when all CD4/CD8-depleted mice were euthanized, although they were healthy at the
266 time. We used a second engineered cell line, PDAC$^{IL6\text{-}LUC}$, which expressed luciferase, to
267 measure tumor burden over time. Both OT-PDAC$^{IL6\text{-}LUC}$ longitudinal data and OT-PDAC^{IL6}
268 endpoint tumor mass data show that CD4/CD8 depletion prevents tumor clearance (**Figure**
269 **3B-C, Figure S7A-D**). Histological evaluation by a board-certified pathologist found tumor
270 present in 10/10 CD4/CD8-depleted mice and in 1/8 IgG control mice (**Figure 3D**). This was
271 supported by *Il6*-transgene qPCR data and plasma IL-6 levels, which showed no elevation of
272 IL-6 in 6/8 IgG-treated PDAC mice (**Figure 3E-F**). We conclude that CD4 and CD8 T cells are
273 necessary for OT-PDAC^{IL6} tumor clearance.

274 Because we previously saw recovery of wasting phenotypes in OT-PDAC^{IL6} mice as the tumor
275 resolved, we also investigated cachexia resolution in T cell-depleted mice. CD4/CD8 depletion
276 prevented body mass recovery and led to sustained muscle wasting, as evidenced by
277 decreased muscle mass and increased atrophy-related gene expression (*Trim63, Fbxo32*)
278 (**Figure 3G-I**). The recovery in wasting is therefore directly associated with immune-mediated
279 tumor clearance.

280 **OT-PDAC^{IL6} induces a durable T cell response to OT-PDAC^{Parental} tumors.** Given the
281 dependency of the anti-OT-PDAC^{IL6} response on T cells, which are known to elicit
282 immunologic memory, we hypothesized that OT-PDAC^{IL6} tumors would generate a durable
283 immune response that would protect mice in the case of a second tumor exposure. We first
284 tested this hypothesis in a cohort of mice that had recovered from sham surgery or OT-
285 PDAC^{IL6} for over two months and rechallenged mice with OT-PDAC$^{parental\text{-}LUC}$ (luciferase-
286 expressing) at 76 days after initial surgery (**Figure 4A**). Sham-recovered mice implanted with
287 PDAC$^{parental\text{-}LUC}$ reached euthanasia criteria 13-14 days post rechallenge implantation. There
288 were no deaths during rechallenge in the OT-PDAC^{IL6}-recovered group (**Figure 4B**). Tumor
289 burden measured longitudinally by IVIS and terminally (in sham-recovered mice only) revealed
290 significant tumor growth only in sham-recovered mice (**Figure 4C-D, Figure S8A**). Sham-
291 recovered mice also lost more body mass than OT-PDAC^{IL6}-recovered mice during
292 rechallenge (**Figure 4E**). These data indicate that the potent anti-tumor immune response
293 elicited by high concentrations of IL-6 is durable and not dependent on coincident
294 supraphysiologic IL-6 levels. We then used CD4/CD8 antibody depletion to determine whether
295 the tumor clearance during rechallenge was indeed T-cell-mediated. In this study, all mice
296 recovered from OT-PDAC^{IL6} for 26 days before starting antibody treatment and were given
297 sham surgery or implanted with OT-PDAC^{parental} tumors on day 28. We monitored mice for 12
298 days, until CD4/CD8-depleted mice reached humane euthanasia criteria (**Figure 4F**). We
299 confirmed that clearance of the rechallenge OT-PDAC^{parental} tumor is dependent on T cells,
300 which were effectively depleted by the antibody treatment (**Figure 4G-I**). Furthermore, we
301 confirmed that CD4/CD8-depletion does not result in outgrowth of potentially covert PDAC^{IL6}
302 cells, as there was no tumor present in the OT-PDAC^{IL6}-recovered, sham-rechallenged,

303 CD4/CD8-depleted mice (**Figure 4G**). These data show that the T cell response induced by
304 OT-PDAC^{IL6} provides durable protection against molecularly similar PDAC tumor growth.

305 **DISCUSSION**

306 Our model of PDAC IL-6 overexpression induces a robust, rapid, and durable anti-tumor T cell
307 response that is accompanied by rapid and severe wasting, which recovers as the tumor is
308 cleared. Although IL-6 is traditionally viewed as a negative actor in pancreatic cancer [1-4], we
309 provide evidence that supraphysiologic levels of IL-6 are sufficient to induce an anti-tumor
310 immune landscape in the pancreas characterized by: increased lymphoid aggregate formation,
311 elevated CD4^{+} T cells, and decreased Foxp3^{+} Treg cells.

312 Unlike cancer types that are now successfully treated with immunotherapy, survival rates for
313 PDAC patients have increased very slowly over the past decade[15]. PDAC is highly
314 immunosuppressive, causing immunotherapies, such as checkpoint blockade, to be ineffective
315 clinically [16]. Previous work indicates that enhancing T-cell activation using exogenous agents,
316 such as agonistic anti-CD40 antibody, improves response to checkpoint blockade therapies
317 and PDAC tumor regression[9]. Our work provides a basis for pursuing IL-6 as an alternative
318 method to improve T-cell response.

319 Our work raises a fundamental contradiction regarding the role of IL-6 in PDAC. We propose
320 that the effect of IL-6 on PDAC growth is pleiotropic and concentration-dependent. At low
321 concentrations, IL-6 aids tumor development via signaling directly on neoplastic cells to drive
322 transformation and growth. At supraphysiologic concentrations seen in OT-PDAC^{IL6} tumor-
323 bearing mice, IL-6 stimulates an anti-tumor immune response. Circulating levels are
324 approximately 100 times higher than what we detect in OT-PDAC^{parental} mice, and we presume

325 that local concentrations in the pancreas are even higher. We can infer that tumor-derived IL-6
326 is the initiating signal for T-cell accumulation and eventual tumor clearance, however, the
327 precise manner in which IL-6 mediates this remains unknown. In addition to increased
328 numbers of tumor-infiltrating T cells, we detected increased NK cells, increased neutrophils,
329 and decreased Treg cells intratumorally. It is possible that IL-6, which is a known
330 immunomodulatory cytokine, impacts multiple cell populations simultaneously to orchestrate
331 an anti-tumor immune microenvironment[17].

332 Although we initially developed the OT-PDAC^{IL6} model to study the effects of IL-6 on cancer
333 cachexia, we have now discovered a novel role for IL-6 to induce a robust anti-tumor T-cell
334 response in PDAC. Our data support the widely-accepted notion that IL-6 induces acutely
335 negative effects, as evidenced by rapid body mass loss of 10-15% in OT-PDAC^{IL6} mice
336 (**Figure 1H**). From a reductionist perspective, this model will open doors to understanding IL-6-
337 mediated T-cell activation in PDAC and the intricacies of cachexia resolution after PDAC tumor
338 clearance. Future work will focus on identifying the immune subpopulations that integrate IL-6
339 signaling into a T-cell response, with the goal of identifying targetable drivers of the anti-tumor
340 response. This will be clinically meaningful as leaning on high-dose IL-6, a known driver of
341 cachexia, is likely dangerous for already vulnerable patients with PDAC.

342 **ACKNOWLEDGEMENTS**

343 We thank all members of the Aaron Grossberg, Robert Eil, and Katelyn Byrne labs for their
344 helpful discussion and suggestions. We also acknowledge the expert technical assistance by
345 staff in the Advanced Multiscale Microscopy Shared Resource and Histopathology Shared
346 Resource. Author contributions are: Conceptualization, PCAW, AQB, RE, and AJG.
347 Methodology, PCAW, AQB, KTB, RE, AJG. Validation, PCAW, AQB, HM, XZ, JD, MM, PRL,

PD. Formal Analysis, PCAW, AQB, HM, XZ, JD, PD, GDS, AJG. Investigation, PCAW, AQB, HM, XZ, JD, MM, PRL, PD, MM, GDS. Writing—Original Draft, PCAW. Writing – Review and Editing, PCAW, AQB, KTB, RE, AJG. Visualization, PCAW, AQB, PD. Supervision, RE, AJG. Project Administration, RE, AJG. Funding Acquisition, RE, AJG. All authors approved this manuscript.

Funding: This work was supported by the National Cancer Institute (AJG: K08CA245188, R37CA280692, R01CA264133; RE: K08CA256179), the Brenden Colson Center for Pancreatic Care, the Oregon Pancreas Tissue Registry, the Histopathology Shared Resource for pathology studies (University Shared Resource Program at Oregon Health and Sciences University and the Knight Cancer Institute (P30 CA069533 and P30 CA069533 13S5)), the OHSU Flow Cytometry Shared Resource (OHSU Knight Cancer Institute NCI Cancer Center Support Grant P30CA069533), and the Advanced Multiscale Microscopy Shared Resource (OHSU Knight Cancer Institute, NIH P30 CA069533). RE was also supported by grants from the American Association of Cancer Research, ASCO, and Pancreatic Cancer Action Network.

364 **REFERENCES**

365 1 Corcoran, R. B. *et al.* STAT3 plays a critical role in KRAS-induced pancreatic
366 tumorigenesis. *Cancer research* **71**, 5020-5029 (2011).
367 2 Suh, S.-Y. *et al.* Interleukin-6 but not tumour necrosis factor-alpha predicts survival in
368 patients with advanced cancer. *Supportive Care in Cancer* **21**, 3071-3077 (2013).
369 3 Rupert, J. E. *et al.* Tumor-derived IL-6 and trans-signaling among tumor, fat, and
370 muscle mediate pancreatic cancer cachexia. *Journal of Experimental Medicine* **218**,
371 e20190450 (2021).
372 4 Razidlo, G. L., Burton, K. M. & McNiven, M. A. Interleukin-6 promotes pancreatic cancer
373 cell migration by rapidly activating the small GTPase CDC42. *Journal of Biological*
374 *Chemistry* **293**, 11143-11153 (2018).
375 5 Flint, T. R. *et al.* Tumor-induced IL-6 reprograms host metabolism to suppress anti-
376 tumor immunity. *Cell metabolism* **24**, 672-684 (2016).
377 6 Arneson-Wissink, P. C. *et al.* Hepatic signal transducer and activator of transcription-3
378 signalling drives early-stage pancreatic cancer cachexia via suppressed ketogenesis.
379 *Journal of Cachexia, Sarcopenia and Muscle* (2024).
380 7 Zhang, Y. *et al.* Interleukin-6 is required for pancreatic cancer progression by promoting
381 MAPK signaling activation and oxidative stress resistance. *Cancer research* **73**, 6359-
382 6374 (2013).
383 8 Foley, K. *et al.* Semaphorin 3D autocrine signaling mediates the metastatic role of
384 annexin A2 in pancreatic cancer. *Science signaling* **8**, ra77-ra77 (2015).
385 9 Winograd, R. *et al.* Induction of T-cell immunity overcomes complete resistance to PD-1
386 and CTLA-4 blockade and improves survival in pancreatic carcinoma. *Cancer*
387 *immunology research* **3**, 399-411 (2015).

388 10 Beatty, G. L., Eghbali, S. & Kim, R. Deploying immunotherapy in pancreatic cancer:
389 defining mechanisms of response and resistance. *American Society of Clinical*
390 *Oncology Educational Book* **37**, 267-278 (2017).
391 11 Byrne, K. T. & Vonderheide, R. H. CD40 stimulation obviates innate sensors and drives
392 T cell immunity in cancer. *Cell reports* **15**, 2719-2732 (2016).
393 12 Ino, Y. *et al.* Immune cell infiltration as an indicator of the immune microenvironment of
394 pancreatic cancer. *British journal of cancer* **108**, 914-923 (2013).
395 13 Hiraoka, N. *et al.* Intratumoral tertiary lymphoid organ is a favourable prognosticator in
396 patients with pancreatic cancer. *British journal of cancer* **112**, 1782-1790 (2015).
397 14 Sautès-Fridman, C., Petitprez, F., Calderaro, J. & Fridman, W. H. Tertiary lymphoid
398 structures in the era of cancer immunotherapy. *Nature Reviews Cancer* **19**, 307-325
399 (2019).
400 15 Siegel, R. L., Miller, K. D., Wagle, N. S. & Jemal, A. Cancer statistics, 2023. *CA: a*
401 *cancer journal for clinicians* **73**, 17-48 (2023).
402 16 Hilmi, M. *et al.* The immunological landscape in pancreatic ductal adenocarcinoma and
403 overcoming resistance to immunotherapy. *The Lancet Gastroenterology & Hepatology*
404 (2023).
405 17 Soler, M. F., Abaurrea, A., Azcoaga, P., Araujo, A. M. & Caffarel, M. M. New
406 perspectives in cancer immunotherapy: targeting IL-6 cytokine family. *Journal for*
407 *ImmunoTherapy of Cancer* **11** (2023).
408 18 Michaelis, K. A. *et al.* Establishment and characterization of a novel murine model of
409 pancreatic cancer cachexia. *Journal of cachexia, sarcopenia and muscle* **8**, 824-838
410 (2017).

411 19 Eil, R. *et al.* Ionic immune suppression within the tumour microenvironment limits T cell
412 effector function. *Nature* **537**, 539-543 (2016).
413 20 Liu, F. & Whitton, J. L. Cutting edge: re-evaluating the in vivo cytokine responses of
414 CD8+ T cells during primary and secondary viral infections. *The Journal of Immunology*
415 **174**, 5936-5940 (2005).

416

417

418 **FIGURES AND FIGURE LEGENDS**

Figure 1

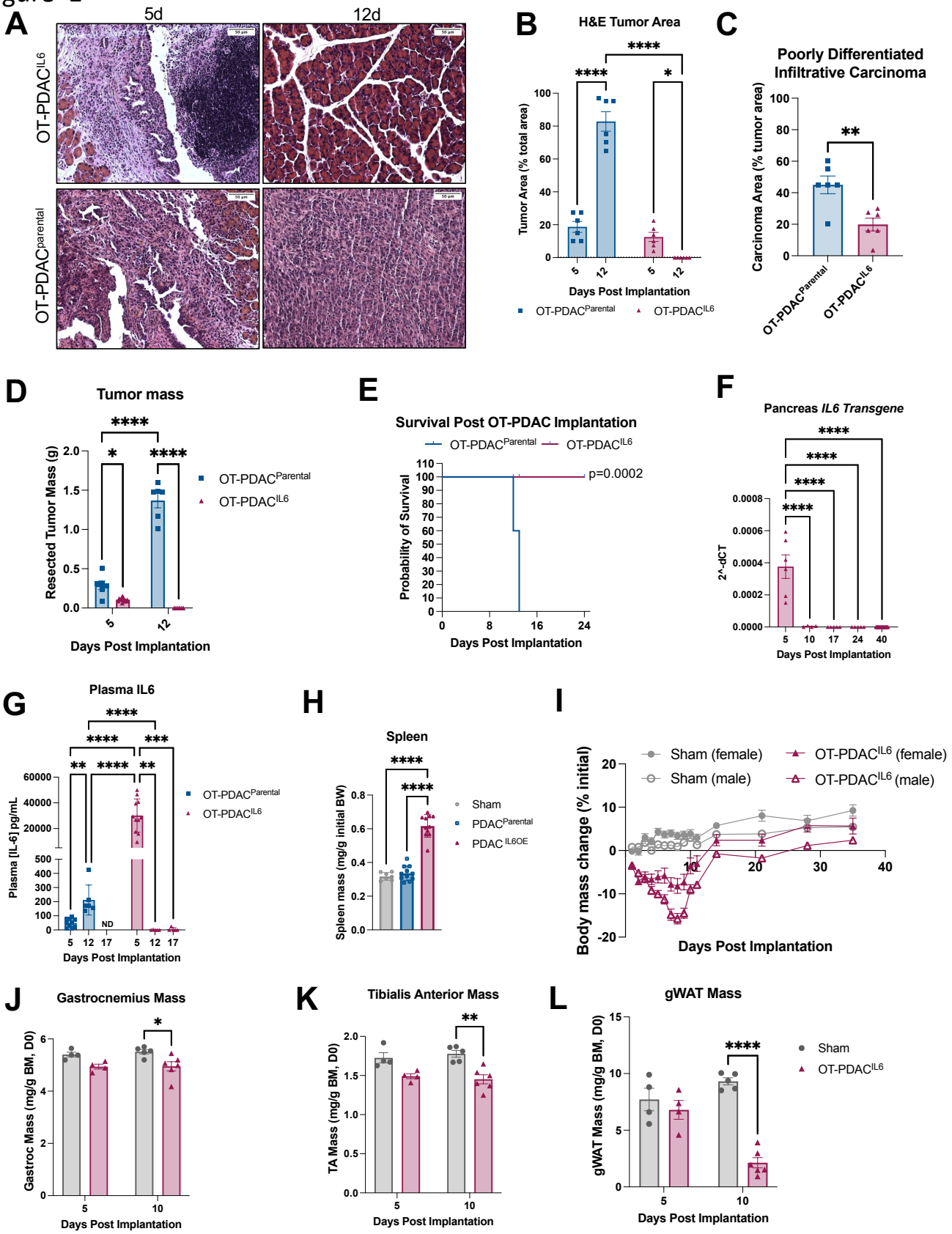
A
5d
12d
OT-PDAC^IL6
OT-PDAC^parental
B
H&E Tumor Area
Tumor Area (% total area)
Days Post Implantation
OT-PDAC^Parental
OT-PDAC^IL6
C
Poorly Differentiated Infiltrative Carcinoma
Carcinoma Area (% tumor area)
OT-PDAC^Parental
OT-PDAC^IL6
D
Tumor mass
Resected Tumor Mass (g)
Days Post Implantation
OT-PDAC^Parental
OT-PDAC^IL6
E
Survival Post OT-PDAC Implantation
OT-PDAC^Parental
OT-PDAC^IL6
p=0.0002
Probability of Survival
Days Post Implantation
F
Pancreas IL6 Transgene
2^-dCT
Days Post Implantation
G
Plasma IL6
Plasma [IL-6] pg/mL
ND
Days Post Implantation
OT-PDAC^Parental
OT-PDAC^IL6
H
Spleen
Spleen mass (mg/g initial BW)
Sham
PDAC^Parental
PDAC^IL6OE
I
Sham (female)
Sham (male)
OT-PDAC^IL6 (female)
OT-PDAC^IL6 (male)
Body mass change (% initial)
Days Post Implantation
J
Gastrocnemius Mass
Gastroc Mass (mg/g BM, D0)
Days Post Implantation
K
Tibialis Anterior Mass
TA Mass (mg/g BM, D0)
Days Post Implantation
L
gWAT Mass
gWAT Mass (mg/g BM, D0)
Sham
OT-PDAC^IL6
Days Post Implantation

419

Figure 1: Tumor-specific IL6 overexpression induces spontaneous tumor clearance and cachexia recovery. (A) Representative pancreas cross sections at 5 (left) and 10 days (right) from OT-PDAC^{IL6} (top) and OT-PDAC^{parental} (bottom) tumor implantation. Scale bars represent 50 um (top) and 100 um (bottom). (B) Tumor area as a percent of total tissue area at 5 and 12 days, quantified by board-certified pathologist. (C) Percentage of tumor area classified as poorly-differentiated, infiltrative carcinoma at 5 days by board-certified pathologist. (D) Tumor mass at 5 and 12 days. (B-D) N = 3 male, 3 female mice per group. (E) Survival comparison of OT-PDAC^{Parental} and OT-PDAC^{IL6}. OT-PDAC^{IL6} were euthanized for study endpoint at 24 days, but had not reached humane euthanasia criteria. N = 4 female, 6 male PDAC^{IL6}, 1 female, 4 male PDAC^{parental} mice. Statistically tested with Log-rank (Mantel-Cox) test. (F) Expression of *Il6 transgene* expression, measured by qPCR at 5 (N = 3 male, 3 female), 10 (N = 6 male), 17 (N = 3 male, 2 female), 24 (N = 3 male, 2 female), and 40 (N = 16 male, 16 female) days. Statistically tested with One-way ANOVA with Tukey correction for multiple comparisons. (G) Plasma IL6 measured by ELISA at 5 (N = 10 male PDAC^{Parental}, 11 male PDAC^{IL6}), 12(N = 3 male, 3 female PDAC^{Parental}, 3 male, 2 female PDAC^{IL6}), and 17 (N = 2 male, 3 female PDAC^{IL6}) days. Statistically tested with 2-way ANOVA main effects only with Tukey correction for multiple comparisons. (H) Spleen mass at 5 days. N = 6 male mice per group. (I) Body mass change as a percentage of initial body mass over time. N = 8 male, 8 female mice per group. Statistically tested with 3-way ANOVA. $p<0.0001$ for Time, Sex, Tumor Status, Time x Sex, Time x Tumor Status. $p=0.0002$ for Sex x Tumor Status. $p= 0.2900$ for Time x Sex x Tumor Status. (J) Gastrocnemius muscle mass normalized to initial body mass. (K) Tibialis anterior muscle mass normalized to initial body mass. (L) gonadal white adipose tissue (gWAT) mass normalized to initial body mass. (J-L) 5d N = 1 female, 3 male mice per group. 10d N = 6 male PDAC, 5 male sham mice. Error bars represent SEM. Unless otherwise noted, 2x2 studies were statistically tested with a full effects model 2-way ANOVA and Sidak multiple comparisons test. 2-group analysis tested with unpaired t-test. **** $p<0.0001$, ***$p<0.001$, **$p<0.01$, *$p<0.05$.

Figure 2

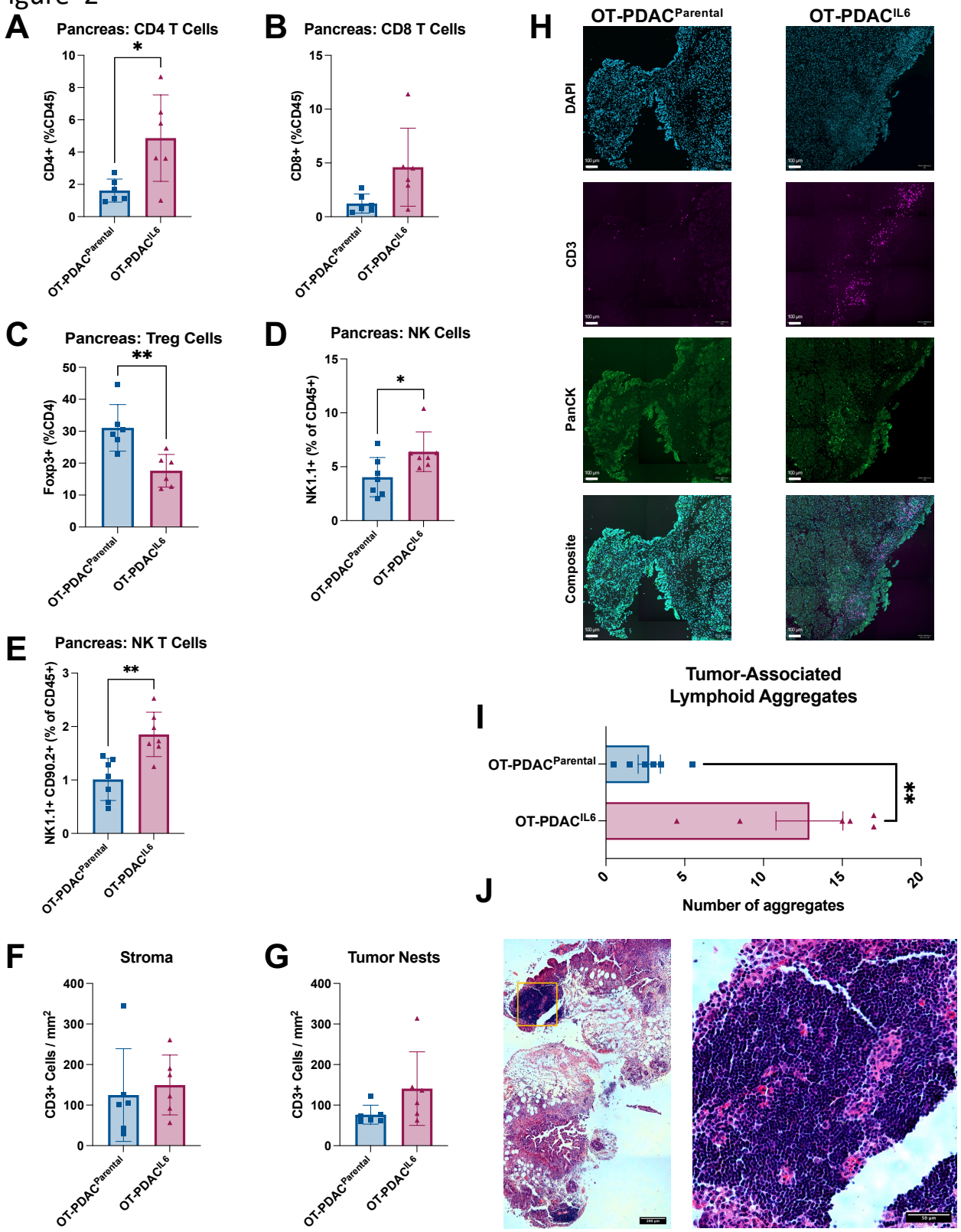
A
Pancreas: CD4 T Cells
CD4+ (%CD45)
OT-PDACParental
OT-PDACIL6
B
Pancreas: CD8 T Cells
CD8+ (%CD45)
C
Pancreas: Treg Cells
Foxp3+ (%CD4)
D
Pancreas: NK Cells
NK1.1+ (% of CD45+)
E
Pancreas: NK T Cells
NK1.1+ CD90.2+ (% of CD45+)
F
Stroma
CD3+ Cells / mm2
G
Tumor Nests
H
OT-PDACParental
OT-PDACIL6
DAPI
CD3
PanCK
Composite
I
Tumor-Associated Lymphoid Aggregates
Number of aggregates
J

447

448 **Figure 2: OT-PDAC^{IL6} induces lymphocytic anti-tumor immune response.** (A-E) Intra-
449 tumoral immune cell populations from pancreas at 5 days: (A) CD4^{+} T cells, (B) CD8^{+} T cells,
450 (C) Foxp3^{+} T regulatory cells, (D) NK1.1^{+} Natural Killer cells, (E) NK1.1^{+}/CD90.2^{+} NK T cells.
451 (A-C) N = 6 male mice per group. (D-E) N = 4 female, 3 male mice per group. (F-G) CD3^{+} cells
452 counted per mm^{2} of stroma (F) or tumor nests (G) in immunofluorescence stained pancreas
453 tissues. N = 3 male, 3 female mice per group. (H) representative images of CD3^{+} T cell
454 infiltration in tumor and associated stroma of OT-PDAC^{parental} (left) and OT-PDAC^{IL6} (right)
455 mice. Tissues were stained with DAPI (blue), CD3 (magenta), and Pancytokeratin (PanCK,
456 green). (scale bars = 100 um) (I) Pathologist-evaluated number of tumor-associated lymphoid
457 aggregates in H&E stained pancreas cross sections from tissue collected at 5 days. N = 3
458 male, 3 female mice per group. (J) Representative H&E image of lymphoid aggregates
459 adjacent to tumor and stroma in OT-PDAC^{IL6} pancreas (left) and magnified image of lymphoid
460 aggregate (right). Area of magnification is denoted on left image with orange box. Error bars
461 represent SEM. 2-group analysis tested with unpaired t-test. **** $p<0.0001$, ***$p<0.001$,
462 **$p<0.01$, *$p<0.05$.

Figure 3

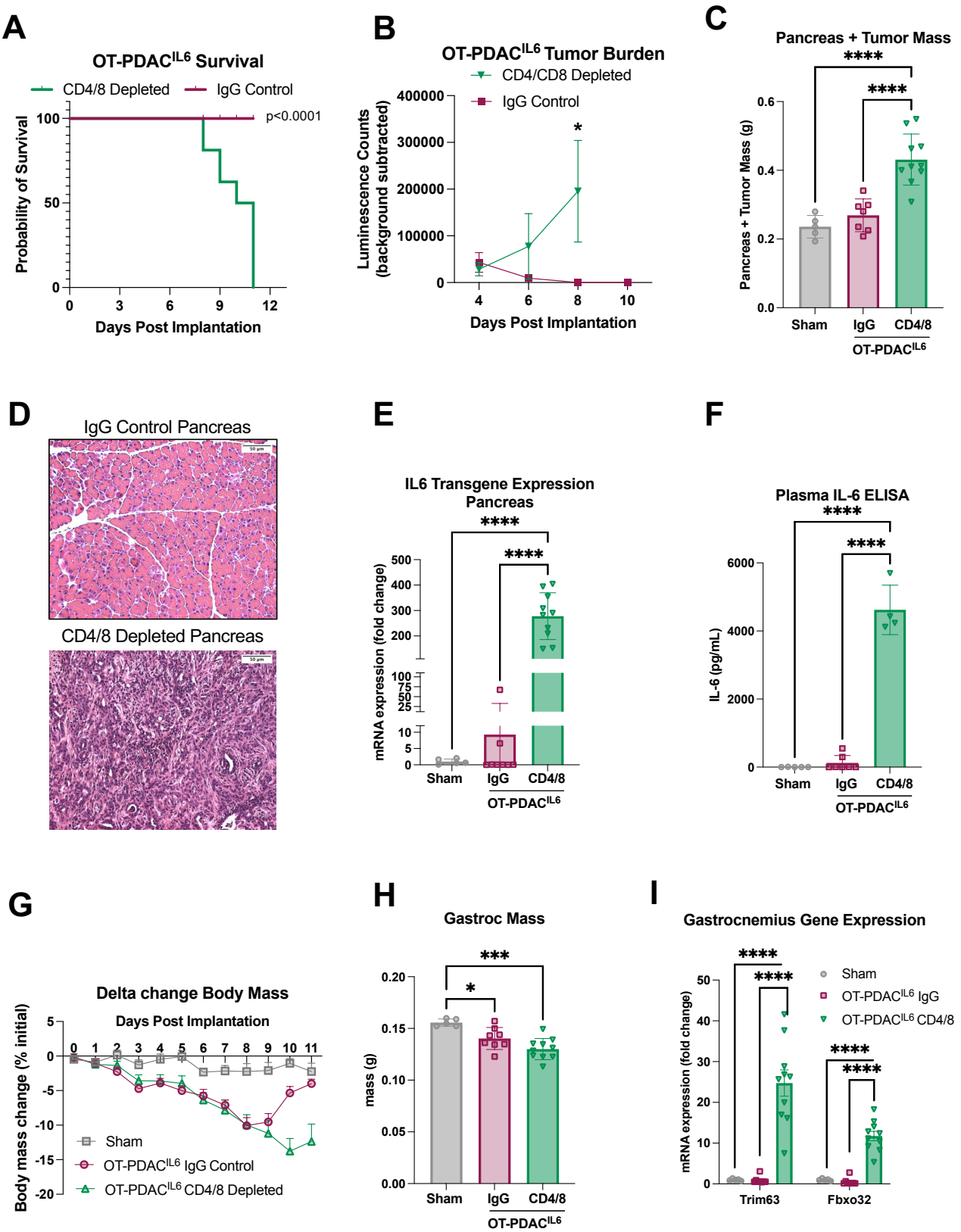
A
OT-PDAC^{IL6} Survival
CD4/8 Depleted
IgG Control
p<0.0001
Probability of Survival
Days Post Implantation
B
OT-PDAC^{IL6} Tumor Burden
CD4/CD8 Depleted
IgG Control
Luminescence Counts (background subtracted)
Days Post Implantation
C
Pancreas + Tumor Mass
Pancreas + Tumor Mass (g)
Sham
IgG
CD4/8
OT-PDAC^{IL6}
D
IgG Control Pancreas
CD4/8 Depleted Pancreas
E
IL6 Transgene Expression Pancreas
mRNA expression (fold change)
Sham
IgG
CD4/8
OT-PDAC^{IL6}
F
Plasma IL-6 ELISA
IL-6 (pg/mL)
Sham
IgG
CD4/8
OT-PDAC^{IL6}
G
Delta change Body Mass
Days Post Implantation
Body mass change (% initial)
Sham
OT-PDAC^{IL6} IgG Control
OT-PDAC^{IL6} CD4/8 Depleted
H
Gastroc Mass
mass (g)
Sham
IgG
CD4/8
OT-PDAC^{IL6}
I
Gastrocnemius Gene Expression
mRNA expression (fold change)
Sham
OT-PDAC^{IL6} IgG
OT-PDAC^{IL6} CD4/8
Trim63
Fbxo32

463

Figure 3: CD4$^+$ and CD8$^+$ T cells are necessary for OT-PDAC^{IL6} tumor clearance. (A) Survival comparison of OT-PDAC^{IL6} mice given CD4/CD8 depletion or IgG control antibodies. Statistically tested with Log-rank (Mantel-Cox) test. (B) OT-PDAC$^{IL6\text{-}LUC}$ tumor growth, measured by IVIS imaging. Statistically tested with 2-way ANOVA, for time points with representation from both groups, with Šídák multiple testing correction. (C) Pancreas and tumor mass at endpoint. (D) Representative pancreas cross sections at humane euthanasia endpoint from IgG control (top) and CD4/CD8 depleted (bottom) mice. Scale bars represent 100 um. (E) expression of *Il6 transgene* expression, measured by qPCR. (F) Plasma IL6 measured by ELISA. (G) Body mass change as a percentage of initial body mass over time. Statistically tested with Mixed-effects analysis with repeated measures. $p<0.0001$ for Time and Time x Tumor Status. $p=0.0048$ for Tumor Status. (H) Gastrocnemius muscle mass at humane euthanasia endpoint normalized to initial body mass. (I) Atrophy-related gene expression (*Trim63* and *Fbxo32*) in gastrocnemius muscle, measured by qPCR. All male mice, N = 5 sham, 10 PDAC^{IL6} per antibody treatment group. Error bars represent SEM. 3 group studies were statistically tested with a 1-way ANOVA and Tukey correction for multiple comparisons. **** $p<0.0001$, ***$p<0.001$, **$p<0.01$, *$p<0.05$.

Figure 4

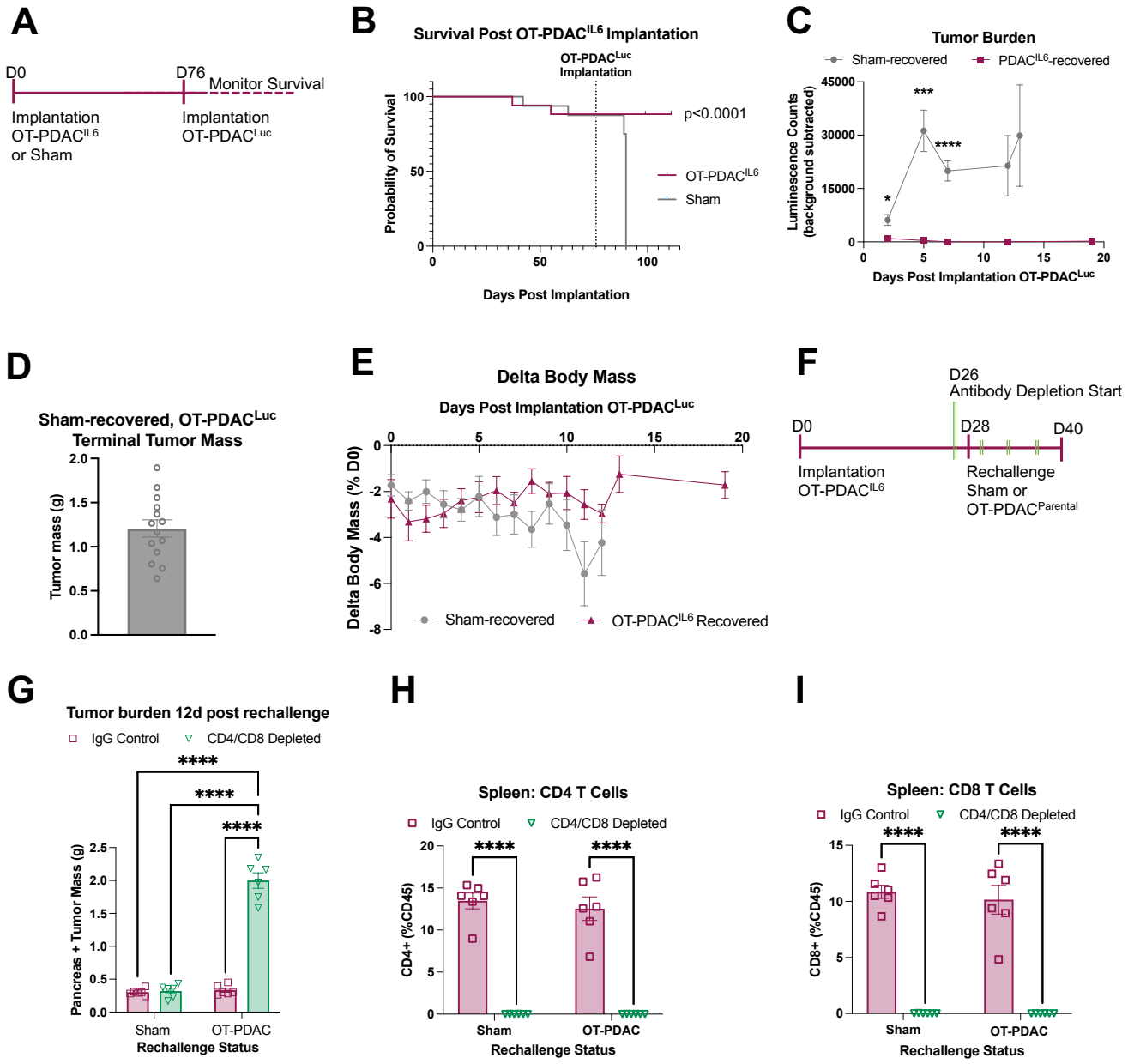

480

481

Figure 4: OT-PDAC^{IL6} induces a durable T cell response to OT-PDAC^{Parental} tumors. (A) Schematic timeline for B-E. Mice were implanted with OT-PDAC^{IL6} or given sham surgery, then all mice were rechallenged with OT-PDAC$^{Parental-LUC}$ after 76 days. (B) Survival comparison of OT-PDAC^{IL6}-recovered and sham-recovered mice. Statistically tested with Log-rank (Mantel-Cox) test. (C) OT-PDAC$^{Parental-LUC}$ tumor growth, measured by IVIS imaging. Statistically tested with mixed effects model and Šídák multiple testing correction, using imputation to match PDAC^{IL6} endpoint with the sham endpoint. (D) Tumor mass at humane euthanasia endpoint for sham-recovered OT-PDAC$^{Parental-LUC}$ tumors. (E) Body mass change as a percentage of initial body mass over time. Statistically tested with mixed effects model and Šídák multiple testing correction at timepoints where both groups were represented. p=0.0435 for Time, p=0.4903 for Tumor Status, p=0.0002 for Time x Tumor Status. (A-E) N = 7 male PDAC^{IL6}, 8 male sham, 7 female PDAC^{IL6}, 6 female sham. (F) Schematic timeline for G-I. Mice were implanted with OT-PDAC^{IL6} or given Sham surgery. 28 days later, mice were rechallenged with OT-PDAC^{Parental}, and given CD4/CD8 depletion or IgG control antibodies beginning on D26 and every 4 days thereafter (denoted with double green lines). (G) Pancreas/tumor mass at 12 days. (H) Intra-tumoral CD4^{+} T cells at 12 days. (I) Intra-tumoral CD8^{+} T cells at 12 days. (F-I) All male mice N = 6 per group. Error bars represent SEM. 2x2 studies were statistically tested with a full effects model 2-way ANOVA and Sidak multiple comparisons test. **** p<0.0001, ***p<0.001, **p<0.01, *p<0.05.